Liquid-Crystalline Elastomer-Nanoparticle Hybrids with Reversible Switch of Magnetic Memory

*Johannes M. Haberl, Antoni Sánchez-Ferrer, Adriana M. Mihut, Hervé Dietsch, Ann M. Hirt, and Raffaele Mezzenga**

Magnetic shape-memory materials are responsive materials with a strong influence of shape changes on the magnetic properties, and vice versa.[1] They offer access to unique applications, including wireless actuators, switches and magnetic valves. To achieve the required mechanical-magnetic coupling, both inorganic materials and polymer-based hybrid systems have been proposed.[1–7] In inorganic materials, the magneto-crystalline anisotropy and the martensitic transformation are typically exploited to induce magnetic reorganization at the phase transition, but the associated elongation and device sizes, are limited to changes of about 10% and to the millimeter range, respectively,[2] which severely limits their use in the mentioned applications. Polymer-based materials, on the other hand, are more efficiently sizeable and recover easily strains beyond 50% by magnetic stimuli.[3,4] However, to achieve magnetic properties of serviceable strength, they require the incorporation of inorganic magnetic particles.[3–8]

To solve this issue and to induce magnetic anisotropy in easy-to-process systems, we propose a new strategy exploiting shape anisotropy of ferrimagnetic nanoparticles in organic-inorganic hybrid materials. The effect of shape-anisotropy is found in soft magnets, such as maghemite, where magneto-crystalline anisotropy is of minor importance and it is explained in terms of the Stoner–Wohlfarth theory.[9,10] In order to achieve full control of the resultant magnetic anisotropy in response to external stimuli, we use a new liquid-crystalline elastomer (LCE) matrix that allows fully reversible changes in shape and physical properties at the smectic-isotropic phase transition,[11] enables shape-memory[12] and can convert external stimuli into mechanical work.[3,5,13–17]

J. M. Haberl, Dr. A. Sánchez-Ferrer, Prof. R. Mezzenga
ETH Zürich
Department of Health Science and Technology
8092 Zürich, Switzerland
E-mail: raffaele.mezzenga@hest.ethz.ch
Dr. A. M. Mihut,[+] Dr. H. Dietsch[++]
Adolphe Merkle Institute and
Fribourg Center for Nanomaterials
University of Fribourg
1723 Marly, Switzerland
Prof. A. M. Hirt
ETH Zürich, Department of Earth Science
8092 Zürich, Switzerland
[+] Present address: Physical Chemistry, Lund University, SE-22210 Lund, Sweden
[++] Present address: BASF SE, Formulation Platform, 67056 Ludwigshafen am Rhein, Germany

DOI: 10.1002/adma.201204406

While in LCE alone output signals beyond shape changes are limited to optical and electrical effects[18–21] and do not include useable magnetic features,[22] the integration of ellipsoidal magnetic nanoparticles (MNs) into LCEs, as proposed in this work, opens new scenarios. The LCE composites allow for accurate control over the global orientation of the MNs and the macroscopic magnetic susceptibility. The resulting material is not only a ductile and inexpensive alternative to magnetic shape memory alloys, but it also greatly expands the scope of materials with magnetic memory and actuation capabilities, bypassing classical limits found in these systems. We show that by stretching the hybrid systems at deformation beyond 200%, with stresses as low as 5 MPa, these new nanocomposites can be used to reversibly store magnetic information that can then be erased at temperatures as low as 80 °C, which are typical conditions of organic materials. We conclude by demonstrating how the anisotropic information is readable in magnetic torque measurements and we point to implications that these materials may have in temperature or strain sensors with magnetic read-out, actuators, magnetic switches and valves.

One major issue in the preparation of hybrid nanocomposites is the suppression of segregation of the nanoparticles from the polymer matrix. Creeping of the polymer matrix and aggregation of the nanoparticles at high temperatures can be avoided when crosslinkable polymers and particles are used; a concept that has already been applied for isotropic networks.[23,24] Therefore we have selected chemically compatible end-functional groups for the two components: hydroxyl groups for the liquid-crystalline polymer and amino groups for the inorganic nanoparticles, which can be mutually crosslinked into a covalent network with a tri-functional isocyanate (see Supporting Information).

For the purpose of generating a strong anisotropic magnetic susceptibility, silica-coated hematite MNs have been synthesized with a narrow and monomodal size distribution[25] and were then redox-processed into silica-coated maghemite.[26] In this study we use new core-shell MNs with a 7:3 maghemite:hematite ratio in the core and an amine-functionalized silica shell (see Supporting Information).

A representative hybrid film with 10 wt% nanoparticles is shown in **Figure 1**a. Due to the presence of iron-oxide-based MNs the sample appears dark brown. The homogeneous distribution and fine dispersion of MNs over the film can be seen in the transmission electron microscopy (TEM) micrograph (Figure 1b; Supporting Information, Figure S1). From statistical analysis on high-resolution TEM images (Figure 1c; Supporting Information, Figure S2,S3) of 100 MNs, the mean core-shell structure is calculated, with a major core axis found to be 310 ± 7 nm and a minor core axis 55 ± 7 nm, which correspond to an aspect ratio of

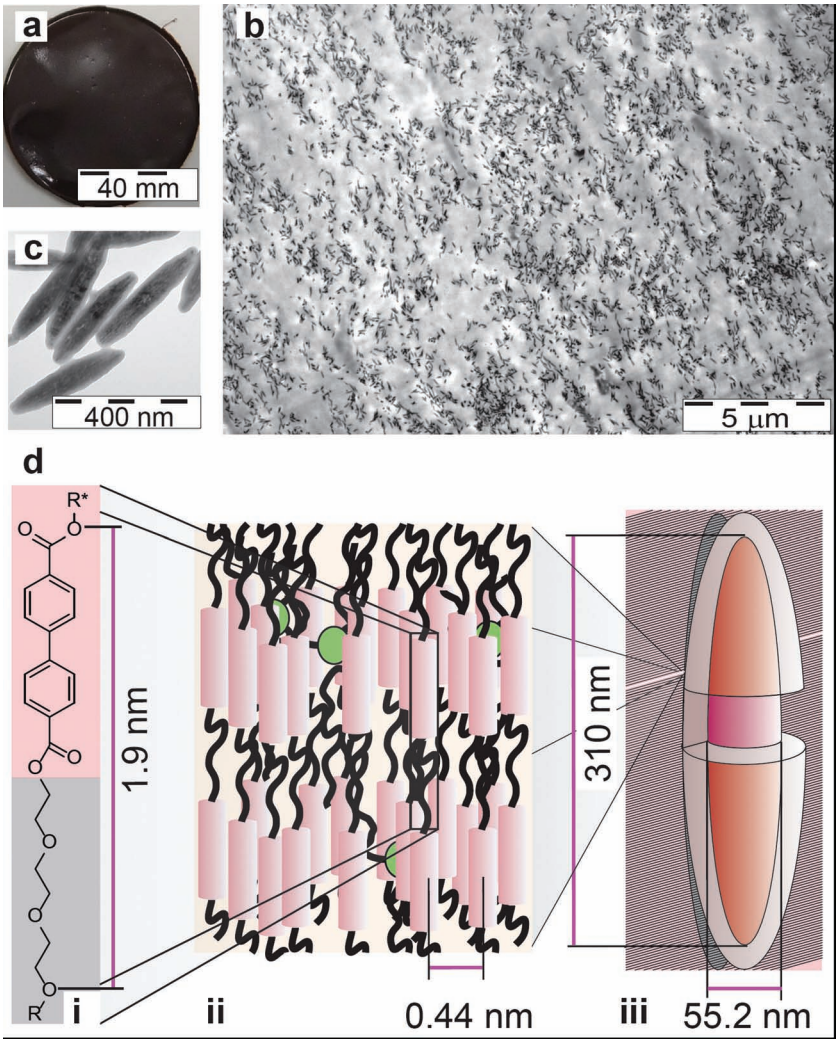

Figure 1. a) Photograph of the liquid-crystalline elastomer-magnetic nanocomposite film. b) TEM micrograph of a stretched sample (80 nm-section microtomed parallel to stretching direction) and c) TEM micrograph of core-shell ellipsoidal nanoparticles. d) Characteristic features for: i) the calamitic repeating unit in the smectic layering of the liquid-crystalline elastomer, ii) the molecular distance in the layers with the crosslinker molecules (green spheres) and iii) the magnetic nanoparticles.

5.6 and the demagnetizing factors $N_{parallel} = 0.048$ and $N_{perpendicular} = 0.476$.[27] The average thicknesses of the silica shell are 22 ± 4 nm along the major axis and 19 ± 2 nm along the minor axis. In Figure 1d a schematic of the microstructure of the hybrid nanocomposite and the length-scales involved are presented.

Differential scanning calorimetry experiments have been performed in order to analyze the phase behavior of the nanocomposites. A glass-transition temperature of T_g = 15 ± 5 °C and a smectic-isotropic transition at T_{SI} = 75 ± 2 °C have been found, respectively.

We then have analyzed the structural and physical properties of the nanocomposite upon stretching, representatively shown for two states. The first state, referred to as "ON", is when the film has been stretched at high temperature to an elastic deformation of $\lambda = 3.2$, which is fixed on cooling down, due to the smectic liquid-crystalline phase. The second state, referred to as "OFF", is when the sample has relaxed back to its original length ($\lambda = 1.0$) due to entropy elasticity, after heating above the clearing temperature T_{SI}. Compared to glassy systems with kinetically driven processes, liquid-crystalline elastomers show all the advantages associated with first order transitions, and thus immediate changes in the mesophase structure at the phase transition together with spontaneous changes in shape.

Small and wide-angle X-ray scattering (SWAXS) experiments for both states ON and OFF have been performed to study the microstructure of the LCE and the MNs orientation distribution (**Figure 2**). 2D-scattering patterns have been taken from the perpendicular directions normal to the film surface (*y*-direction in Figure 2a,c) and normal to the film thickness (x-direction Figure 2b,d). From the evaluation of the WAXS patterns a smectic layering distance of d_l = 1.9 nm with a correlation length of ξ = 24 nm and a mesogen-mesogen distance of d_m = 0.44 nm have been measured. From the azimuthal intensity distribution the orientation distribution of scattering elements and the order parameter:

$$S = {}^1\!/_2 \cdot \langle 3\cos^2\theta - 1 \rangle \quad (1)$$

have been calculated.[28,29] This definition of the order parameter relies on cylindrical symmetry. In cases where cylindrical symmetry is lost with respect to any axis, we still use the definition, but identify the order parameter with an additional asterisk, S^*.

The 2D-WAXS pattern for the OFF state shows a LC polydomain structure without scattering intensity anisotropy (Figure 2a and blue and green curves in Figure 2b). However, the SAXS pattern in the *y*-direction (Figure 2b, red curve) shows two maxima in the azimuthal intensity distribution with the order parameter $S = -0.28$ (calculated around a director in *y*-direction). As the scattering of the reference polymer systems presents no features in this *q*-region (see Supporting Information, Figure S7), these SAXS profiles can be univocally attributed to a planar orientation distribution of the particles parallel to the film surface due to in-plane confinement during the synthesis of the film.

In Figure 2c and Figure 2d the SWAXS patterns and azimuthal scans for the ON states are presented. In the WAXS pattern in *y*-direction (Figure 2c) anisotropic scattering is observed with two maxima in the mesogen distance. These peaks in the azimuthal intensity distribution (blue curve) indicate preferential orientation of the mesogens long axes parallel to the stretching direction with an order parameter $S = 0.70$ (calculated around a director in *z*-direction). Two additional maxima at the layering distance appear perpendicular to the former and indicate

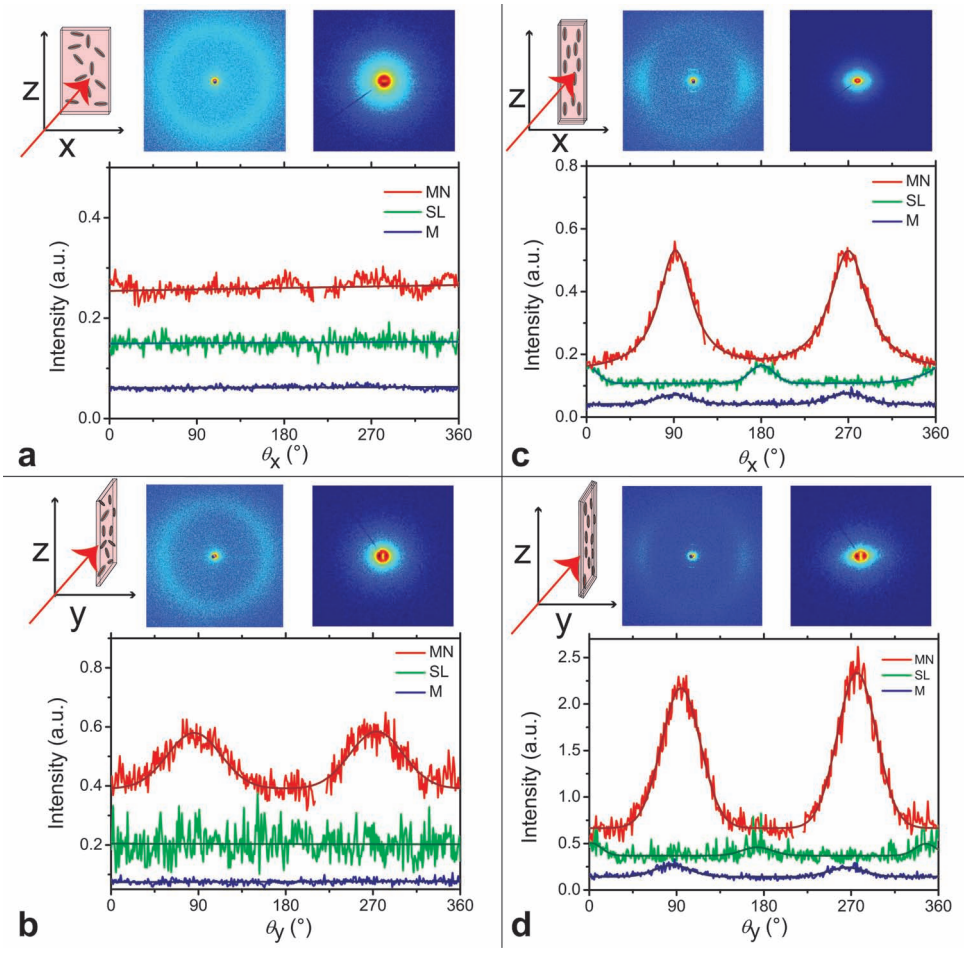

Figure 2. Two-dimensional X-ray scattering patterns in the wide angle (light blue) and small-angle (dark blue) regions for the OFF state after relaxation (a, *y*-direction; b, *x*-direction) and ON state after stretching (c, *y*-direction; d, *x*-direction), with the azimuthal scans at the corresponding correlation lengths of the magnetic nanoparticles short axes (red curve at $q = 0.15–0.25$ nm^{-1}), the smectic layering (green curve at $q = 3.3$ nm^{-1}) and the mesogens (blue curve at $q = 14$ nm^{-1}). Note: the red arrow indicates the X-ray beam direction.

a smectic A phase (green curve). In the SAXS pattern the azimuthal intensity distribution at the characteristic nanoparticle length scale (red curve) shows two intensity maxima that indicate an orientation of the mean particle long axes parallel to the stretching direction with an order parameter $S^* = 0.56$ (calculated around a director in *z*-direction). This is in agreement with an earlier, similar study.[23]

The 2D-WAXS pattern in *x*-direction is shown in Figure 2d. From the azimuthal intensity distribution at the mesogen distance, a degree of order $S = 0.68$ is calculated and the two maxima for the smectic A layering are found consistently with the evaluation in Figure 2c. From the 2D-SAXS pattern, the azimuthal intensity distribution at the MNs characteristic distance (red curve) is evaluated with a corresponding anisotropy quantified by $S^* = 0.69$. This increase in value, compared to Figure 2c, is a direct consequence of the in-plane confinement of the MNs.

From the SWAXS analysis above, we can summarize the restructuring upon stretching for both the liquid-crystalline elastomer and the nanoparticles, which both align the mesogens and the nanoparticles long axes parallel to the strain direction (ON state), while an in-plane isotropic orientation distribution of both liquid crystal domains and nanoparticles is found when the stored deformation is released ($\lambda = 1$, OFF state) (**Figure 3**).

Low-field magnetic susceptibility measurements of the nanocomposite have been performed in order to determine the anisotropic magnetic susceptibility of the sample in the OFF and ON states. In order to remove potential effects from field inhomogeneity the ON sample (with $\lambda = 3.2$) was folded twice, to yield dimensions directly comparable with the OFF sample and allowing measurements under identical geometrical set-up. Both the OFF and ON samples were rotated stepwise around the three axes *x*, *y* and *z*, and the 2nd-rank susceptibility tensors have been calculated. The normalized eigenvalues K_{ij}(OFF) = {1.04, 1.04, 0.91} and K'_{ij}(ON) = {1.19, 0.95, 0.86} are obtained with residuals of 0.5%. For the OFF state, K_1 and K_2 were identical as expected from the isotropic 2D-SAXS pattern (Figure 2a). K_3 was about 14% lower, which is the result of the in-plane confinement of the nanoparticles (Figure 2b). For the ON state, K'_1 is 25% higher than K'_2 as a consequence of the reorientation process of the MNs along the stretching direction, which leads to a deformation of the bulk susceptibility tensor with expansion in *z*-direction.

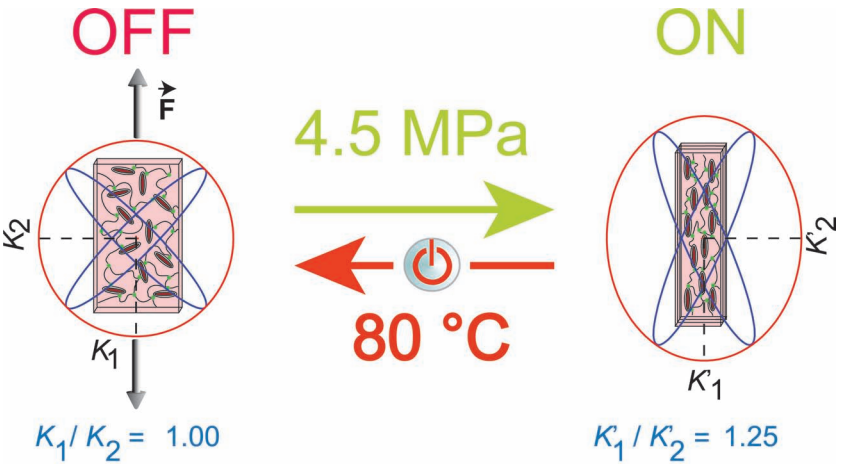

Figure 3. Control over low-field magnetic susceptibility with the two states, OFF and ON. On the left, the random distribution of magnetic nanoparticles in the liquid-crystalline elastomer nanocomposite in the OFF state after relaxation, characterized by an order parameter $S^* = 0$ and the corresponding low-field anisotropic magnetic susceptibility $K_1/K_2 = 1$. The colored arrows indicate triggering (green) and release (red) of the anisotropic magnetic susceptibility. On the right, the liquid-crystalline elastomer nanocomposite and the oriented magnetic nanoparticles in the ON state after stretching, characterized by an order parameter $S^* = 0.56$ and the corresponding low-field anisotropic magnetic susceptibility $K'_1/K'_2 = 1.25$.

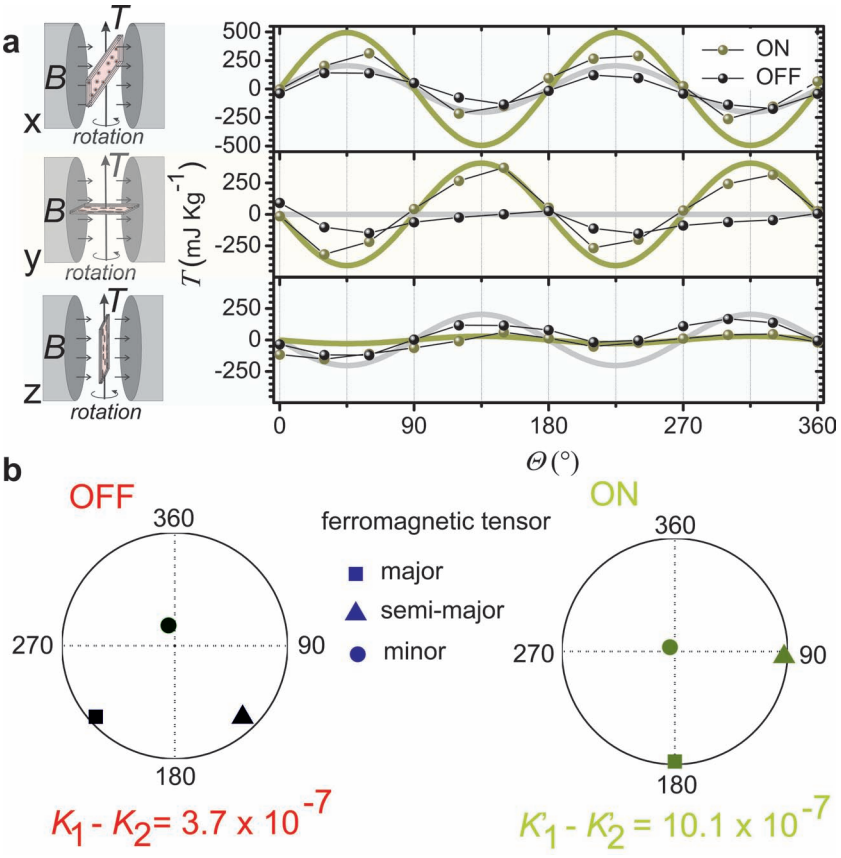

Figure 4. a) The magnetic torque experiment set-up[30] and data of the nanocomposite at the magnetic field $B = 1.4$ T in x, y and z direction for the ON (green dots) and the OFF (black dots) states, together with the corresponding theoretical curves (solid lines). b) The stereogram of the ferromagnetic tensor for the OFF and ON states with the eigenvalues difference of the major and the semi-major axes.

In Figure 3, the xz-plane of the low-field magnetic susceptibility measurements for the OFF and ON states are represented with red ellipses. In order to compare the measurements of the susceptibilities with theoretical expectations, we apply a Stoner–Wohlfarth model,[10] which supports the presence of an anisotropic magnetic susceptibility $K'_1/K'_2 \approx 2.1$ (see Supporting Information), consistently with the measurements. The deviation of the theoretical anisotropic magnetic susceptibility compared to the measured one ($K'_1/K'_2 = 1.25$) is expected and, as discussed below, in agreement with the results from high-field magnetic measurements and attributed to the effects that arise from the 30 wt-% hematite content in the MNs. The model-assumption of a particle magnetization obeying the global energy minima (Supporting Information, Figure S4), multigrain structures and surface effects in the particles, and interparticle magnetic dipole coupling may further contribute to this overestimation.

To get further details on the magnetic structure we performed complementary high-field magnetic torque measurements (**Figure 4**). During these experiments the magnetization of the MNs is saturated and aligned with respect to the external field. Any tilt angle θ between the long axis of a MN and the magnetic field generates a torque that is measured and predicted (solid line) for the entire nanocomposite following:

$$\tau = \mu_0/2 \cdot V \cdot \left| N_{\text{parallel}} - N_{\text{perpendicular}} \right| \cdot M_s^2 \cdot S^* \cdot \sin(2\Theta) \qquad (2)$$

with the volume of iron-oxide $V = 3.95 \times 10^{-11}$ m^3, the magnetic constant $\mu_0 = 4\pi \times 10^{-7}$ NA^{-2}, the saturation Magnetization $M_s = 120$ kA m^{-1}, $N_{\text{parallel}} - N_{\text{perpendicular}}$ and S^* defined as above, and Θ the angle between the sample and the magnetic field (Figure 4a).[31,32]

The torque in the x-direction for the OFF state shows a 2Θ-signal periodicity which fits well with the theoretical curve, using $S = -0.28$. Moreover, the signal strength in the ON state maintains the same 2Θ-periodicity, but increases in magnitude, in agreement with the corresponding theoretical expectation for $S^* = 0.69$. The overestimation compared to the measurement is due to the value S^*, which overestimates the order after stretching due to the in-plane confinement of the MNs in y-direction before stretching, an effect contributing to S^* but not to S, that is significant in both "OFF" and "ON".

For the measurement in y-direction a very weak signal is found for the OFF state. Since

theoretically for $S = 0$ no torque is expected, this suggests that there is a contribution from the 30 wt% of hematite in the MNs. Hematite has a strong magnetocystalline anisotropy that would be oriented in this direction.[25] The measurement for the ON state shows a strong periodical 2Θ-signal, which corresponds perfectly to the theoretical calculation, using $S^* = 0.56$.

In z-direction the OFF state also has a 2Θ-periodicity and the intensity agrees with the prediction for the measured $S = -0.28$. For the ON state the torque decreases, because stretching has produced a decrease in the population of MNs peaked around the equatorial direction, the only component which contributes to torque in this case. The theoretical curve is computed with an order parameter $S^* = -0.04$ that has been obtained from the X-ray scattering experiment in the z-direction (Supporting Information, Figure S5).

The resulting tensors of the torque measurements are shown in Figure 4b. The stereogram from OFF constitutes an oblate-like tensor around z with a small eigenvalue difference of $K_1 - K_2 = 3.7 \times 10^{-7}$ that is not oriented with respect to the previous stretching direction, whereas the ON ensemble is represented by a tensor with the eigenvalue difference $K'_1 - K'_2 = 10.1 \cdot 10^{-7}$ and K_1 lies in the stretching direction. Interestingly, the OFF state is not completely isotropic in the $K_1 - K_2$ plane, which is the origin of the non-zero torque that is observed in the y-direction. The minor axis corresponds to the in-plane orientation distribution that has also been confirmed by SWAXS experiments. Thus the deformation of the material is correctly measurable with both low and high magnetic fields.

We have presented a new class of hybrid nanocomposites, where the unique combination of liquid-crystalline elastomers and anisotropic magnetic nanoparticles is exploited to generate a material with magnetic memory that can be reversibly stored by mechanical deformation and erased by heating to moderate temperatures. The resulting shape-memory materials allow manipulation of magnetic properties of inorganic materials *via* the control of parameters that are typical of soft materials, and thus greatly expand the scope of magnetic materials. As stored magnetic information is reachable by simple measurements, such as magnetic torque, and can be reversibly tuned, the route presented here increases possibilities in the design of actuators beyond presently achievable imprinted magnetic geometries,[33] and shows great promise in strain sensing devices and magnetic information storage applications.

Supporting Information

Supporting Information is available from the Wiley Online Library or from the author.

Acknowledgements

The research was financed by the NRP 62 of the Swiss SNF. We gratefully acknowledge I. Usov for assistance with the calculations.

Received: October 23, 2012
Revised: December 11, 2012
Published online: January 29, 2013

[1] J. Ma, I. Karaman, *Science* **2010**, *327*, 1468–1469.
[2] A. Sozinov, A. A. Likhachev, N. Lanska, K. Ullako, *Appl. Phys. Lett.* **2002**, *80*, 1746–1748.
[3] A. Kaiser, M. Winkler, S. Krause, H. Finkelmann, A. M. Schmidt, *J. Mater. Chem.* **2009**, *19*, 538–543.
[4] R. Mohr, K. Kratz, T. Weigel, M. Licka-Gabor, M. Moneke, A. Lendlein, *Proc. Natl. Acad. Sci. USA* **2006**, *103*, 3540–3545
[5] I. Levine, R. B. Zvi, M. Winkler, A. M. Schmidt, M. Gottlieb, *Macromol. Symp.* **2010**, *291–292*, 278–286.
[6] A. M. Schmidt, *Macromol. Rapid Commun.* **2006**, *27*, 1168–1172.
[7] U. N. Kumar, K. Kratz, M. Behl, A. Lendlein, *Polym. Exp. Lett.* **2012**, No. *1*, 26–40.
[8] Y. Zhou, N. Sharma, P. Deshmukh, R. K. Lakhman, M. Jain, R. M. Kasi, *J. Am. Chem. Soc.* **2012**, *134*, 1630–1641.
[9] R. C. O'Handley, in *Modern Magnetic Materials: Principles and Applications*, Wiley-Interscience, New York **1999**.
[10] E. C. Stoner, E. P. Wohlfarth, *Phil. Trans. R. Soc. A* **1948**, *240*, 599–642.
[11] M. Warner, E. M. Terentjev, in *Liquid Crystal Elastomers*, Vol. *2*, Oxford University Press, Oxford, UK **2007**.
[12] I. A. Rousseau, P. T. Mather, *J. Am. Chem. Soc.* **2003**, *125*, 15300–15301.
[13] J. Küpfer, H. Finkelmann, *Makromol. Chem., Rapid Commun.* **1991**, *12*, 717–726.
[14] H. Finkelmann, E. Nishikawa, G. G. Pareira, M. Warner, *Phys. Rev. Lett.* **2001**, *87*, 011501.
[15] V. Ahir, E. M. Terentjev, *Nat. Mater.* **2005**, *4*, 491–495.
[16] W. Lehmann, H. Skupin, C. Tolksdorf, E. Gebhard, R. Zentel, P. Krüger, M. Lösche, F. Kremer, *Nature* **2001**, *410*, 447–449.
[17] A. Sanchez-Ferrer, A. Merekalov, H. Finkelmann, *Macromol. Rapid. Commun.* **2011**, *32*, 671–678.
[18] W. Kossak, P. Papadopoulus, P. Heinze, H. Finkelmann, F. Kremer, *Macromolecules* **2010**, *43*, 7532–7539.
[19] H. Finkelmann, S. T. Kim, A. Muñoz, P. Palffy-Muhoray, B. Taheri, *Adv. Mater.* **2001**, *13*, 1069.
[20] J. Harden, M. Chambers, R. Verduzco, P. Luchette, J. T. Gleeson, S. Sprunt, A. Jáckli, *Appl. Phys. Lett.* **2010**, *96*, 102907.
[21] P. Heinze, H. Finkelmann, *Macromolecules* **2010**, *43*, 6655–6665.
[22] A. Buka, W. H. de Jeu, *Physique* **1982**, *43*, 361–367.
[23] A. Sánchez-Ferrer, R. Mezzenga, H. Dietsch, *Macromol. Chem. Phys.* **2011**, *212*, 627–634.
[24] A. Sánchez-Ferrer, M. Reufer, R. Mezzenga, P. Schurtenberger, H. Dietsch, *Nanotechnology* **2010**, *21*, 185603.
[25] M. Reufer, H. Dietsch, U. Gasser, B. Groberty, A. M. Hirt, V. K. Malik, P. Schurtenberger, *J. Phys.: Condens. Matter.* **2011**, *23*, 065102.
[26] V. Städele, U. Gasser, H. Dietsch, *Soft Matter* **2012**, *8*, 4427–4431.
[27] J. A. Osborn, *Phys. Rev.* **1945**, *67*, 351–357.
[28] G. R. Mitchell, A. Windle, in *Orientation in Liquid Crystal Polymers*, Elsevier Applied Science, London, New York **1988**.
[29] R. Lovell, G. R. Mitchell, *Acta. Crystallogr. Sect. A* **1981**, *37*, 135–137.
[30] F. Bergmüller, C. Bärlocher, B. Geyer, M. Grieder, F. Heller, P. Zweifel, *Meas. Sci. Technol.* **1994**, *5*, 1466–1470.
[31] Y. Watanabe, *J. Compos. Mater.* **2002**, *36*, 915–923.
[32] J. J. Abbot, O. Ergeneman, M. O. Kummer, A. M. Hirt, B. J. Nelson, *IEEE Trans. Robotics* **2007**, *6*, 1247–1252.
[33] J. Kim, S. E. Chung, S.-E. Choi, H. Lee, J. Kim, S. Kwon, *Nat. Mater.* **2011**, *10*, 747–752.